RSC Advances

ROYAL SOCIETY OF CHEMISTRY

www.rsc.org/advances

Journal Name

ARTICLE

CFD Simulations on Effect of Catalysts on Hydrodeoxygenation of Bio-Oil

Received 00th January 20xx,
Accepted 00th January 20xx

DOI: 10.1039/x0xx00000x

www.rsc.org/

Anjani R.K. Gollakota,[a] Malladi D. Subramanyam,[a] Nanda Kishore,*[a] and Sai Gu[b]

Bio-oil derived from lignocellulose biomass is an emerging alternative resource of the conventional fossil fuel. However, the so-obtained unprocessed bio oil is oxy-rich, low pH and contains high moisture which suppresses the heating value and the mixing with conventional fuel is not compatible. Hence studies on the upgradation of bio oil using catalytic hydrodeoxygenation (HDO) are becoming prominent in the recent years. This study present computational fluid dynamics (CFD) based simulation results on the effects of catalysts (Pt/Al_2O_3, $Ni\text{-}Mo/Al_2O_3$, $Co\text{-}Mo/Al_2O_3$) on upgradation of bio oil using hydrodeoxygenation process in an ebullated bed reactor. These numerical simulations are performed using Eulerian multiphase flow module available in commercial CFD based solver, ANSYS Fluent 14.5. Prior to obtaining new results, the present numerical solution methodology is validated by reproducing some of the experimental results on upgradation of bio oil available in the literature. Further, the influence of weightily hour space velocities (WHSV), operating temperature, and pressure inside the reactor for the different catalysts on the performance of HDO for bio oil upgradation in ebullated bed reactor are delineated. It is observed that the gaseous stream products are higher in the presence of Pt/Al_2O_3 catalyst, phenols are higher by the use of $Ni\text{-}Mo/Al_2O_3$ and higher aromatics are obtained with $Co\text{-}Mo/Al_2O_3$ catalyst. Finally a comparison among the mass fraction of the individual species of three phases with respect to different catalysts for various combinations of WHSV, temperature and pressure values are presented.

Keywords: Bio-oil upgradation, Ebullated bed, Hydrodeoxygenation, Lumped kinetic parameters, Weight hourly space velocity, Catalyst.

Introduction

Demand for the energy is increasing globally and expected to be double in the coming years due to population growth and various developments in society. The major source of energy generation to meet the present necessities is from fossil fuels. This energy generation resulting the emission of CO_2 leading to the problems related to climate changes, such as global warming. So, globally there is a challenge to counterbalance the environmental protection and generation of alternative source of fuel to suffice the demand. To address these challenges World is stimulated to use the renewable energies such as wind, solar, biomass and hydroelectricity. Among which biofuels are emerging as a promising solution and alternative source of energy due to the sustainability and CO_2 neutral resources. These bio fuels are derived from the biological carbon fixation and are mainly resulted from biomass feed stocks. Some interesting facts about bio mass feed stocks are free from sulphur, nitrogen and ash thus the emissions are also free from SO_x, NO_x, CO_2 emissions. Because of diversity, bio-fuels are classified into various sections and named as renewable advanced bio fuels or next generation sustainable fuels. This classification is majorly depending on the type of feed stock, conversion technology, product formed and carbon source. Bioethanol and bio-diesel are the first generation biofuels derived from biomass, whereas, second generation biofuels are derived from lignocellulosic biomass but the major obstacle is to degrade the biomass. Therefore the third generation biofuels are derived from microalgae and cyanobacteria. The bio oil that is obtained from the pyrolysis of lignocellulosic biomass is unstable due to its instability, high content of water, low pH, high viscosity, low heating value, and highly corrosive. According to Oasmaa *et al.*[1], the produced bio-oil made of 300 different organic compounds consists of mostly (20-30 wt. %) water, (15-30 wt. %) lignin fragments, (10-20 wt. %) aldehydes, (10-15 wt. %) carboxylic acids, (5-10 wt. %) carbohydrates, (2-5 wt. %) phenols, (1-4 wt. %) furfurals, (2-5 wt. %) alcohols and (1-5 wt. %) ketones. In order to overcome the deleterious properties of bio mass pyrolysis oil, the upgrading process is required before its application. Currently there are various techniques available to upgrade bio-oils into transportation fuels. They are catalytic hydrodeoxygenation (Furimsky[2]), zeolite upgrading (Adjaye and Bakshi[3]), catalytic cracking (Hew *et al.*[4]), super critical technology (Tang *et al.*[5], Zhang *et al.*[6]) and emulsification (Bridgwater[7]).

[a] Department of Chemical Engineering, Indian Institute of Technology Guwahati, Assam – 781039, India.
[b] Centre for Biofuel, School of Energy, Environmental and Agrifood, Cranfield University, United Kingdom.

Research activities on the upgradation of bio-oils using HDO have started in 1970's. The first review on the accomplishment of upgradation process of bio-oil through HDO for the past 25 years is successfully explained by Furimsky[2]. Other pioneering work of Furimsky[8] explained the chemistry, difficulties in determining rate constants, problems associated with the presence of oxygen, growing concern of upgrading coal and biomass derived fuels in details. This led to the paradigm shift of research towards the techniques pertaining to upgradation. Oyama[9] reported that the HDO process is similar to hydrodenitrogenation (HDN) but 10 times smarter than the later technique over vanadium nitride catalysts. Maggi and Delmon[10] published a review, and discussed various aspects related to the catalytic chemistry, kinetics, and mechanisms of HDO reactions using various model oxygenated compounds inline to the review of Furimsky[2]. Senol[11], Mahfud[12] and Gutierrez *et al*.[13] explained the process of removal of oxygen from bio oil using HDO under high pressure in the presence of suitable catalysts such as Cobalt-Molybdenum or Nickel-Molybdenum. Mahfud[12] presented the reaction stoichiometry of the HDO process and reported that HDO is efficient in terms of carbon efficiency saturates C=C, C=O bonds and aromatic rings while removing oxygen in presence of H_2 and catalysts, resulted for the production of the renewable liquid fuels like gasoline and diesel. Further, extension to the earlier studies Gutierraz *et al*.[14] reported that the bio oil upgradation by HDO require relatively high pressures in the range of (7-20 MPa) to convert some of the compounds of bio-oils that have a low HDO reactivity to O-free products. Further Elliott and Hart[15] conducted semi batch HDO experiments using acetic acid and furfural to represent pyrolysis products from hemi-cellulose and cellulose, respectively in the absence of catalyst. The authors reported the formation of a solid polymeric material from furfural at 250 °C. Using Ru/C as catalyst and acetic acid as feed, they observed negligible conversions at low temperatures (<200 °C) and strong gas production at high temperatures (>250 °C). Their approach resulted in a reduction of the oxygen content from 41.3 %wt. to 20-27.0 %wt.[16-18] Wildschut *et al.*[19] conducted HDO experiments in an autoclave using glucose and cellulobiose as model compounds for the sugar fraction of pyrolysis oil. They concluded that, during HDO of these model compounds using a ruthenium on carbon (Ru/C) catalyst, the catalytic hydrotreatment route is preferred over the thermal decomposition that would lead to the formation of tar/solids (humins). The main products observed were polyols and gas products (mostly methane). Later Wildschut *et al.*[20] found that there is no formation of benzene in the product on the HDO reaction of phenol over Ru/C catalyst. Recent results of Widschut *et al.*[20]; Li and Huber[21]; and de Miguel Mercader *et al.*[22] indicate HDO process removes the oxygen under high pressures with a zeolite catalyst in the form of CO, CO_2 and H_2O. Further, the aqueous-phase reforming have been developed and tested for the bio-oil upgrading by Taarning *et al.*[23] Another historical review of Mortensen *et al.*[24] on the catalytic upgradation of bio-oil to engine fuels and suggested two different paths for the upgradation process as hydrodeoxygenation and zeolite cracking. The author reported that the HDO process majorly occurs in the range of temperature of 310-350 °C and pressure of 10-140 bar. They suggested a replacement of catalyst suitable for HDO which includes sulphide catalyst and noble catalyst with base metal catalyst which was supported by Wang *et al.*[25] Also HDO is found to be the suitable way to produce synthetic fuels of acceptable grade for current infrastructure and also its usage as platform chemical to co-process in refinery units[22,26-30]. Bridgwater[7] presented a review on fast pyrolysis of biomass and suggested that the bio refineries are the best possible scope for the bio-fuel upgradation. Recently, Yaseen *et al.*[31] experimentally studied the HDO of fast pyrolysis bio-oils from various feed stocks using carbon-supported catalysts. They concluded that the switch grass bio-oil over Pt/C catalyst performed the best in terms of hydrogen consumption efficiency, deoxygenation efficiency, and types of bio-oil upgraded compounds. The extensive work that has been undertaken over the past 25−30 years in the field of catalytic hydrotreating of biomass derived liquids is thoroughly reviewed by several researches[32-36].

Finally from the aforementioned extensive literature review, it can be concluded that several experimental studies on the upgradation of bio oil using HDO in the presence of suitable catalysts are available in the literature; however, analogous information on the basis of numerical studies are virtually non-existent. Therefore this work is aimed to numerically investigate the performance of HDO process for the upgradation of bio oil in the presence of Pt/Al_2O_3, $Ni\text{-}MO/Al_2O_3$, $Co\text{-}MO/Al_2O_3$ catalysts over wide ranges of WHSV, temperature and pressure using a CFD approach.

Problem Statement and Mathematical Formulation

A schematic representation of the ebullated bed reactor used in the present simulation study is shown in Fig. 1. The height of the reactor is chosen to be 0.813 m and the diameter of the reactor is chosen to be 0.01564 m. The reactor is initially packed with catalyst particles up to 0.508 m of the maximum packing limit height. The conditions for free board and the catalyst bed are specified in terms of volume fraction. The catalyst volume fractions are obtained using:

$$\epsilon = \frac{W_s}{\rho_c A_c h} \qquad (1)$$

where W_s is the weight of the solid fed to the reactor, ρ_c is the density of the catalyst, A_c is the cross section are of the reactor, h is the packing height. The volume fraction of the catalyst in the bed is calculated to be 0.0286 in the case of Pt/Al_2O_3 catalyst and it is 0.75 for $Ni\text{-}Mo/Al_2O_3$, and $Co\text{-}Mo/Al_2O_3$ catalysts. In other words, only volume fraction of 0.0286 (out of the initial maximum packing height of 0.508m) is occupied by the catalyst particles when Pt/Al_2O_3 catalyst is used; and similarly volume fraction of 0.75 is occupied by the catalyst particles when $Ni\text{-}Mo/Al_2O_3$ and $Co\text{-}Mo/Al_2O_3$ catalysts are used. The pine pyrolytic oil consisting of various lumping groups along with hydrogen (H_2) gas is introduced from the bottom of the reactor to pass through the catalyst bed.

The thermo-physical properties of three phases used in the present simulations are listed in Table 1. The oil feed rate and its velocity is calculated based on the value of the weight hourly space velocity which is given by:

$$WHSV = \frac{gram\ of\ pine\ pyrolytic\ oil\ input\ per\ hour}{Gram\ of\ catalyst\ in\ reactor}\ (hr^{-1})$$

For the gas phase inlet conditions, the minimum fluidization velocity of the gas phase is used in the present simulation studies. The bed region is initialized as heterogeneous mixture of solid and gas phases and the gas is fully occupied in freeboard region.

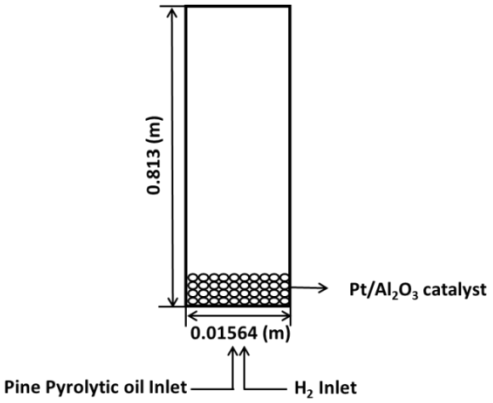

Fig. 1 Schematic representation of ebullated bed reactor for bio-oil upgradation using HDO

Table 1 Thermo-physical properties of the three phases used in the simulation studies

	Compound	ρ (kg/m^3)	μ (Pa.s)	C_p (J/kg.K)	K (W/m.K)
Pine oil	HNV	841.15	0.0009	1833.81	0.127
	LNV	679.5	0.0004	2223.19	0.140
	Phenols	1030	0.1842	1430.00	0.190
	Aromatics	880	0.0008	1699.84	0.131
	Alkane	0.669	0.00001	2222	0.033
Gas	H_2 (Gas)	0.8189	0.000008	14283	0.167
	Water Vapour	0.5542	0.000013	2014	0.0261
Catalyst	Pt/Al_2O_3	21450	0.000017	130	71.6
	$Ni\text{-}Mo/Al_2O_3$	829.75	0.000017	1360.71	0.186
	$Co\text{-}Mo/Al_2O_3$	829.75	0.000017	1243.47	0.2213
	Coke +Ash	375	1.206	850	0.2

In order to obtain the hydrodynamics and performance of upgradation of bio oil, following model equations along with appropriate reaction kinetics are to be solved simultaneously.

The continuity equation for all the three phases.[37]

$$\frac{\partial}{\partial t}(\alpha_q\rho_q) + \nabla.(\alpha_q\rho_q\overrightarrow{v_q}) = 0 \quad (2)$$

Fluid –fluid and fluid-solid momentum equation is given by Alder and Wainwright[38]

$$\frac{\partial}{\partial t}(\alpha_q\rho_q\overrightarrow{v_q}) + \nabla.(\alpha_q\rho_q\overrightarrow{v_q}\overrightarrow{v_q}) = \alpha_q\rho_q\vec{g} + \nabla.\overline{\overline{\tau_q}} - \alpha_q\nabla \mathrm{p} + \sum_{p=1}^{n}\left(K_{pq}(\overrightarrow{v_p} - \overrightarrow{v_q})\right) + \overrightarrow{F_q} \quad (3)$$

$$\frac{\partial}{\partial t}(\alpha_s\rho_s\overrightarrow{v_s}) + \nabla.(\alpha_s\rho_s\overrightarrow{v_s}\overrightarrow{v_s}) = \alpha_s\rho_s\vec{g} + \nabla.\overline{\overline{\tau_s}} - \alpha_s\nabla \mathrm{p} - \nabla p_s + \sum_{l=1}^{n}(K_{ls}(\overrightarrow{v_l} - \overrightarrow{v_s})) \quad (4)$$

Interphase momentum exchange coefficient between liquid and solid phases.[39-41]

$$K_{ls} = C_d\frac{3}{4}\rho_l\frac{\alpha_l\alpha_s}{d_s}|\overrightarrow{u_s} - \overrightarrow{u_l}|\alpha_l^{-2.65} + \frac{150\alpha_s(1-\alpha_l)\mu_l}{\alpha_l{d_s}^2} + \frac{1.75\alpha_s\rho_l(\overrightarrow{u_s}-\overrightarrow{u_l})}{d_s} \quad (5)$$

The drag between the solid and fluid wall is given by Schillar and Naumann[42] as

$$K_{pq} = \frac{\alpha_p\rho_p(1 + 0.15\mathrm{Re}^{0.687})}{\tau_p} \quad (6)$$

The energy conservation equation is given as

$$\frac{\partial}{\partial t}(\alpha_q\rho_q h_q) + \nabla.(\alpha_q\rho_q h_q\overrightarrow{u_q}) = -\alpha_q\frac{\partial_{pq}}{\partial t} + \overline{\overline{\tau_q}}:\nabla\overrightarrow{u_q} - \nabla.\overrightarrow{q_q} + S_q + \sum_{p=1}^{n}\frac{\left(6c_q\alpha_q\alpha_p Nu(T_p - T_q)\right)}{{d_p}^2} \quad (7)$$

Fluid-Fluid interaction is governed by Ranz and Marshall[43] and fluid-solid by Gunn[44]

$$Nu_p = 2.0 + 0.6{Re_p}^{1/2}Pr^{1/3} \quad (8)$$

$$Nu_s = \left(7 - 10\alpha_f + 5\alpha_f^2\right)\left(1 + 0.7Re_s^{0.2}Pr^{1/3}\right) + \left(1.33 - 2.4\alpha_f + 1.2\alpha_f^2\right)Re_s^{0.7} \quad (9)$$

The turbulent kinetic energy (k) for the multiphase is governed by Launder and Spalding.[45]

$$\frac{\partial}{\partial t}(\rho k) + \frac{\partial}{\partial x_i}(\rho k u_i) = \frac{\partial}{\partial x_j}\left[\left(\mu + \frac{\mu_t}{\sigma_k}\right)\frac{\partial k}{\partial x_j}\right] + G_k + G_b - \rho\epsilon - Y_M + S_k \quad (10)$$

The dissipation rate (ε) of the turbulent kinetic energy for all the phases is also explained by Launder and Spalding.[45]

$$\frac{\partial}{\partial t}(\rho\epsilon) + \frac{\partial}{\partial x_i}(\rho\epsilon u_i) = \frac{\partial}{\partial x_j}\left[\left(\mu + \frac{\mu_t}{\sigma_\epsilon}\right)\frac{\partial\epsilon}{\partial x_j}\right] + C_{1\epsilon}(G_k + C_{3\epsilon}G_b) - C_{2\epsilon\rho} - \frac{\epsilon^2}{k} + S_\epsilon \quad (11)$$

$$\frac{3}{2}\left[\frac{\partial}{\partial t}(\rho_s\alpha_s\theta_s) + \nabla.(\rho_s\alpha_s\theta_s\overrightarrow{v_s})\right] = \left(-p_s\bar{\bar{I}} + \bar{\bar{T}}\right):\nabla\overrightarrow{v_s} + \nabla.\left(K_{\theta_s}\nabla\theta_s\right) - \gamma\theta_s + \emptyset_{ls} \quad (12)$$

and finally the diffusion coefficient by Dinag and Gidaspow.[46]

$$K_{\theta_s} = \frac{150\rho_s d_s\sqrt{\theta\pi}}{384(1+e_{ss})g_{0,ss}}\left[1+\frac{6}{5}\alpha_s g_{0,ss}(1+e_s)\right]^2 + 2\rho_s\alpha_s^2 d_s(1+e_{ss})g_{0,ss}\sqrt{\frac{\theta_s}{\pi}} \quad (13)$$

Lumped Kinetic Models

Since there are many species present in both pine pyrolytic oil and its hydrotreated products, the lumping of their constituents together with similar functional groups is a useful approach for studying reaction kinetics. Also the lumped kinetic models give a useful insights and clear understanding in order to quantify the effects of process variables on product yields. In this work, five lumping kinetic model for hydrodeoxygeneation of pyrolytic bio-oil proposed by Sheu *et al.*[47] is used; and the reaction pathway is shown in Fig. 2 and in Table 2.

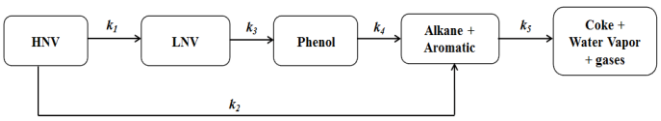

Fig. 2 Reaction Pathways of hydroprocessing of pine pyrolytic oil (Sheu et al.[47])

All these reactions are forward reactions, i.e., they are irreversible and their rate equations are given below:

$$r_1 = -k_1\rho_1 \quad (14)$$

$$r_2 = k_1\rho_1 - k_2\rho_2 - k_3\rho_2 \quad (15)$$

$$r_3 = k_3\rho_2 - k_4\rho_3 \quad (16)$$

$$r_4 = k_2\rho_2 + k_4\rho_3 - k_5\rho_4 \quad (17)$$

$$r_5 = k_5\rho_4 \quad (18)$$

where ρ_1, ρ_2, ρ_3, and ρ_4 are the densities of the heavy non-volatiles, light non volatiles, phenols and alkane aromatics respectively. The reactions pathway follows the forward direction alone without any backward reactions as shown in Table 2 and in Figure 2.

Numerical methodology

The aforementioned model equations for hydrodynamics and reaction kinetics are solved simultaneously by using turbulent flow module available in commercial CFD software ANSYS Fluent 14.5 in double precision mode. The methodology employs a finite volume approach for flow solutions, which is beneficial for local satisfaction of the conservation equations and for relatively coarse grid modelling. As shown in Fig. 1 the velocity inlet and pressure outlet boundary conditions are used for the present simulation studies as the realistic values promotes numerical convergence. For wall boundaries, no slip boundary is applied. A pressure based solver is employed to solve phasic momentum equations, shared pressure, and phasic volume fraction equations in a segregated manner. The phase coupled semi-implicit method for pressure linked equations (PC-SIMPLE) algorithm is implemented which is an extension of the SIMPLE algorithm developed for multiphase flows. In the PC-SIMPLE method, velocities are solved coupled by phases, yet in a segregated manner. A block algebraic multigrid scheme is then used to solve a vector equation of the velocity components of all phases simultaneously. For spatial discretization, a second order upwind scheme is chosen for the momentum equation and QUICK scheme is chosen for volume fractions. The QUICK scheme is based on a weighted average of second-order upwind and central interpolations of the variable. The time step size used for simulation is in the order of 10^{-3}. The structured quadrilateral grid is implemented using hexadral mesh of 12462 nodes. The post processing of the simulation results were performed using CFD post 14.5.

Results and Discussion

Validation

The results on the upgradation of bio-oil using HDO process through numerical approach are virtually non-existent and to the best of our knowledge, only Sheu *et al.*[47] reported the results on upgradation of bio-oil using HDO process in terms of numeric.

Table 2 Lumped kinetic parameters of pine pyrolytic oil due to Sheu *et al.*[47]

	HNV → LNV	HNV → Alkane + Aromatic	LNV → Phenol	Phenol → Alkane + Aromatic	Alkane + Aromatic → H_2O + Gases + Coke
			Pt/Al_2O_3		
Activation Energy, $E_a \times 10^{-7}$ (J/kmol)	7.40	9.18	8.06	6.23	6.96
Arrhenius Constant, A (min^{-1})	3860	75400	8300	950	4000
			$Ni\text{-}Mo/Al_2O_3$		
Activation Energy, $E_a \times 10^{-7}$ (J/kmol)	8.22	10.58	9.04	6.84	7.49
Arrhenius Constant, A (min^{-1})	8800	654000	30600	1920	16400
			$Co\text{-}Mo/Al_2O_3$		
Activation Energy, $E_a \times 10^{-7}$ (J/kmol)	7.45	9.64	8.18	6.90	5.58
Arrhenius Constant, A (min^{-1})	3500	218000	7700	3100	450

Therefore the present numerical solver is validated by comparing the present values of the mass fractions of the lumped species of the upgraded bio-oil phase with the existing experimental results due to Sheu *et al.*[47] and shown in Table 3. The present results are in close proximity with the existing literature values which boosted us the confidence to proceed further in order to check the effects of various catalysts over the wide ranges of temperature, pressure and weight hourly space velocities.

Table 3 Validation of present results at T=623 K, P=8720 kPa and WHSV=2 hr^{-1} with experimental results of Sheu *et al.*[47]

Lumped Fraction	Unprocessed pyrolytic oil (wt.%) [47]	Upgraded pyrolytic oil (wt. %)	
		Experimental (Sheu et al.[47])	Present numerical results
HNV	0.4932	0.2457	0.2102
LNV	0.3690	0.2941	0.4083
Phenol	0.1232	0.1063	0.1552
Alkane +Aromati	0.0146	0.1952	0.1962
Coke+gas +H_2O	0	0.1587	0.000169

Volume Fractions of Upgraded Pine Oil, Catalyst and H_2 Gas

Figures 3-5 show the prototype volume fraction images of all the three phases (i.e., catalyst phase in Figure 3, pyrolytic oil phase in Figure 4 and H_2 gas phase in Figure 5) at T=673 K and P=8720 kPa at WHSV=3 hr^{-1} in the presence of Pt/Al_2O_3 catalyst. It can be noted from the volume fraction of all three phases that these phases expand with the increasing time and reach a limiting maximum permissible height of 0.508 m of the bed. The volume fraction images of the catalyst phase (Figure 3) indicate that the total volume of the catalyst remain constant though they distribute (expand) up to the bed height of 0.508 m. On the other hand, the volume fraction images of upgraded pine oil (Figure 4) increases with the increasing time indicating the change in the composition of their lumped species and attain steady value at larger time values. The volume fraction images of H_2 gas phase (Figure 5) indicate that most of it occupies the free board space; however significant amount of H_2 is also available in the bed region for upgradation of bio-oil. Similarly Figure 6 denotes the steady mass fraction of the lumped species of the upgraded bio-oil obtained by the use of Pt/Al_2O_3 catalyst at WHSV=3 hr^{-1} at T=673 K and P=8720 kPa. The mass fraction images shown in Figure 6 are after the steady state has arrived, that is the bed expansion has ceased and no further change in composition of upgrading bio-oil is observed.

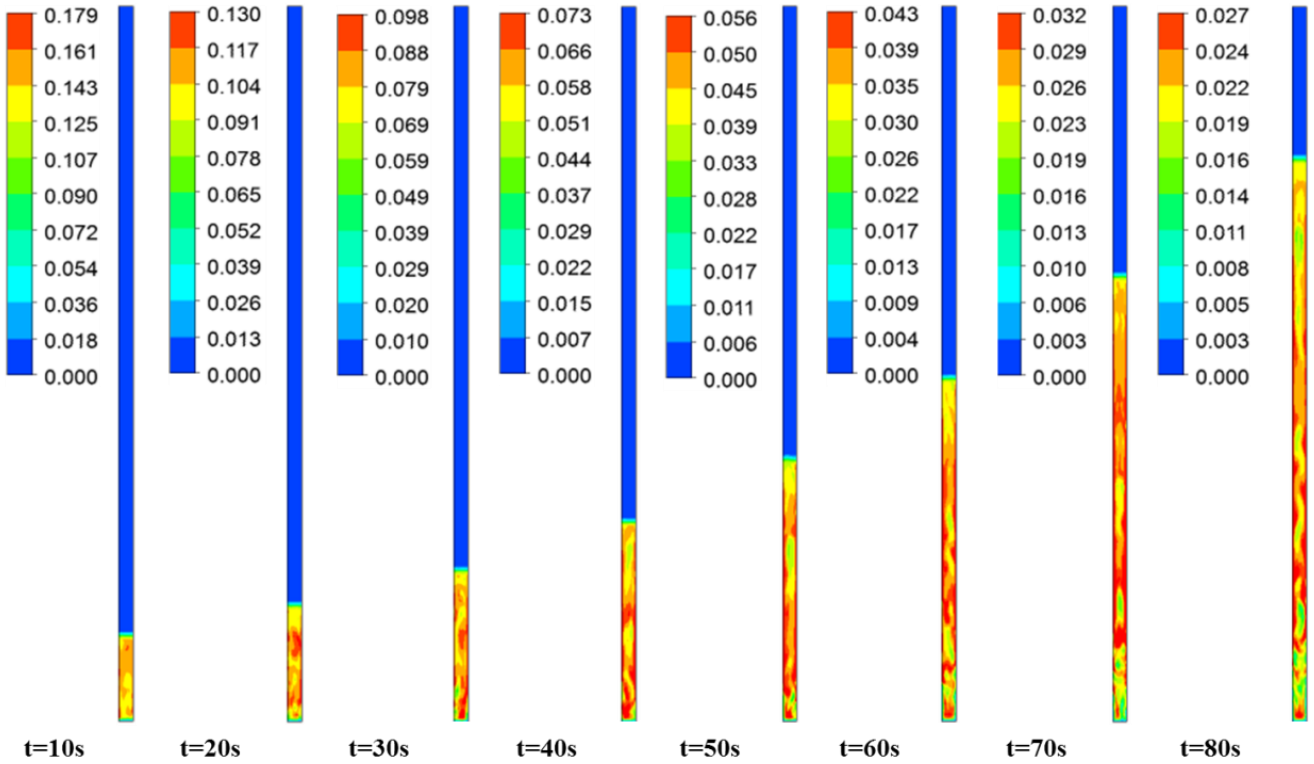

Fig. 3 Expansion of Pt/Al_2O_3 catalyst bed at WHSV=3 hr^{-1}, T=673 K and P=8720 kPa with increasing time.

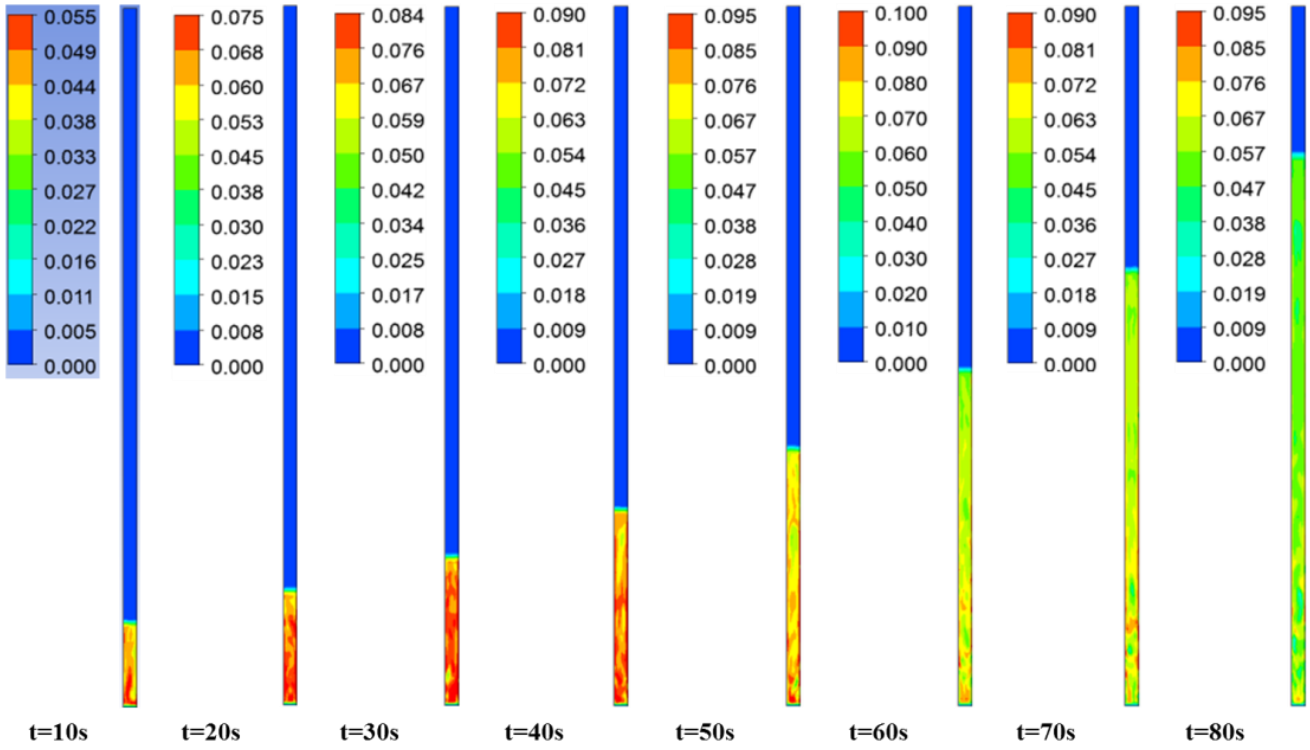

Fig. 4 Volume fraction images of pine pyrolytic oil phase with increasing time at WHSV=3 hr^{-1}, T=673 K and 8720 kPa in presence of Pt/Al_2O_3 catalyst.

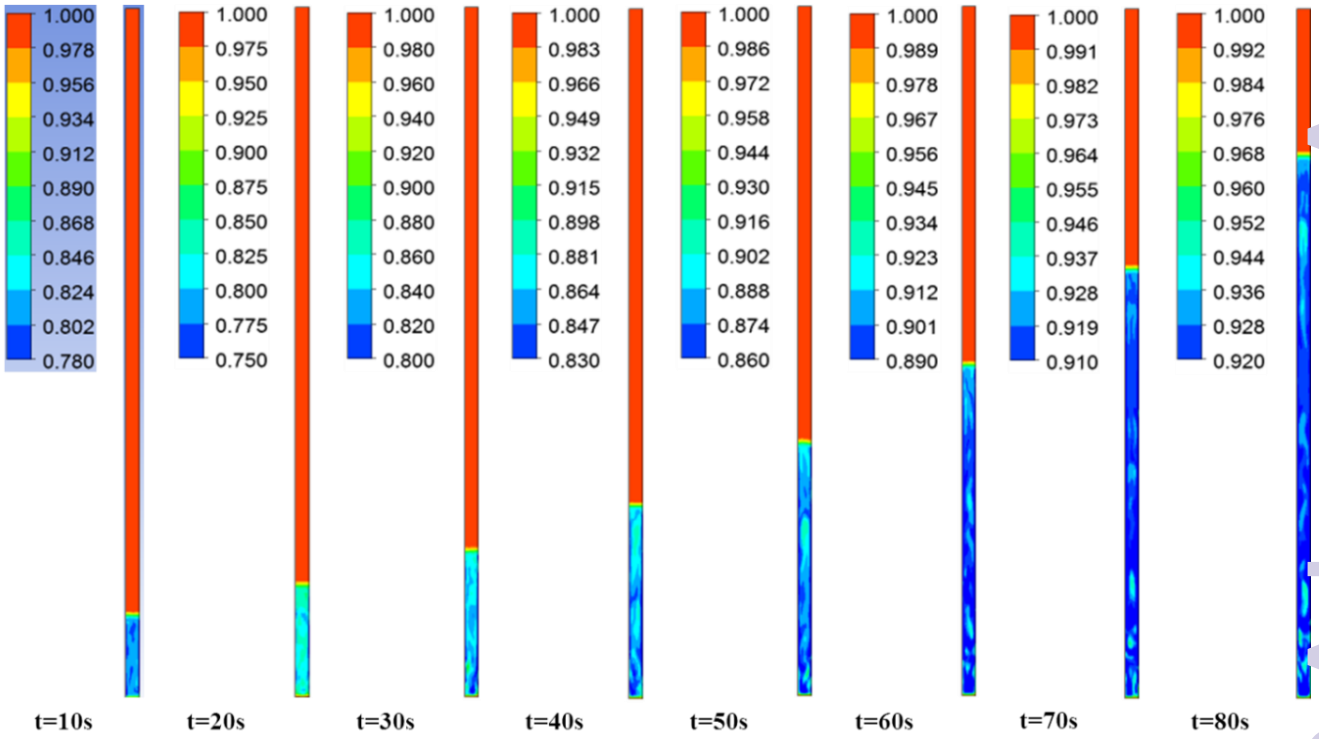

Fig. 5 Volume fraction of the H_2 gas phase with increasing time at WHSV=3 hr^{-1}, T=673 K and 8720 kPa in presence of Pt/Al_2O_3 catalyst.

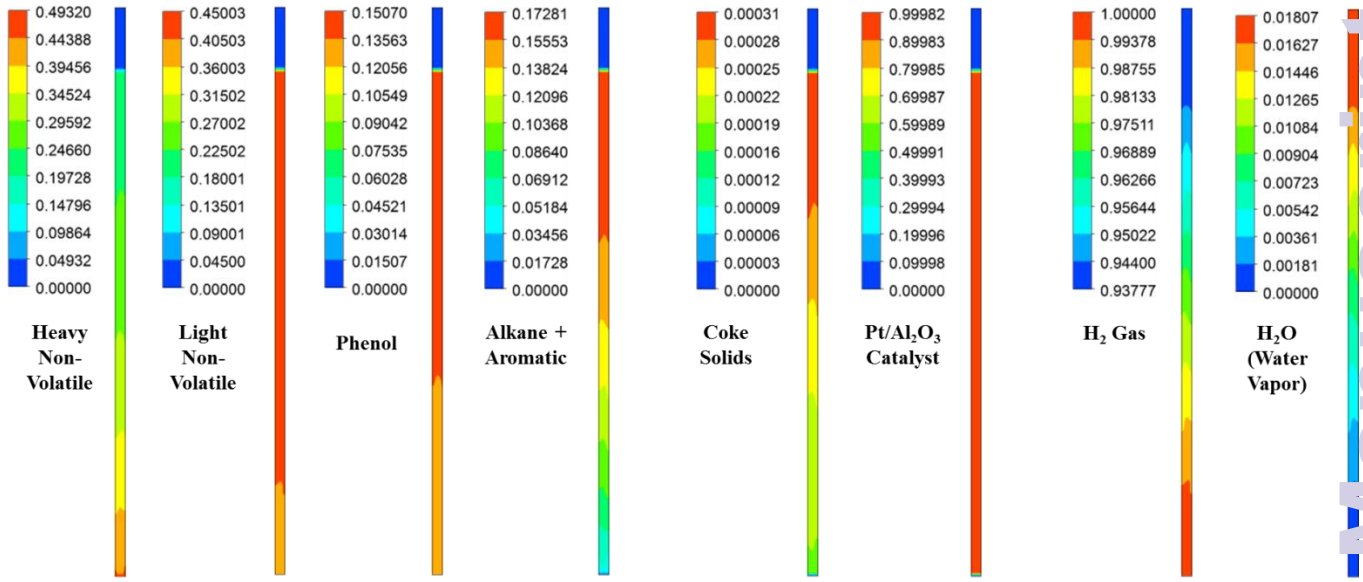

Fig. 6 Steady mass fraction images of lumped species of upgraded pyrolytic oil and those of solid and gas/vapour phases in presence of Pt/Al_2O_3 catalyst at WHSV=3 hr^{-1}, T=673 K and P=8720 kPa

It can be seen from Figure 6 that all lumped species of upgraded bio-oil are expanded within the maximum limit of bed height and their composition in the free board region is zero; however, the H_2 gas escapes into the freeboard region. Also the final steady mass fractions of HNV, LNV, phenols, and alkanes and aromatics in this figure are consistent with the experimental mass fractions reported by Sheu *et al*. [47] From this simulation results it can be said that it is possible to almost completely overcome the coke formation. Also the water vapours (moisture) contents can be reduced to almost a negligible fraction (<2% vol) provided the experimental conditions are maintained exactly same as in the simulations.

Figures 7 – 9 shows the effects of temperature, pressure and WHSV on the volume fraction of catalyst phase, H_2 gas phase and upgraded oil phase in the presence of Pt/Al_2O_3 catalyst (Figure 7), $Ni\text{-}Mo/Al_2O_3$ catalyst (Figure 8) and $Co\text{-}Mo/Al_2O_3$ catalyst (Figure 9). The line legends are same for Figures 7–9; hence they are shown in Figure 8 only.

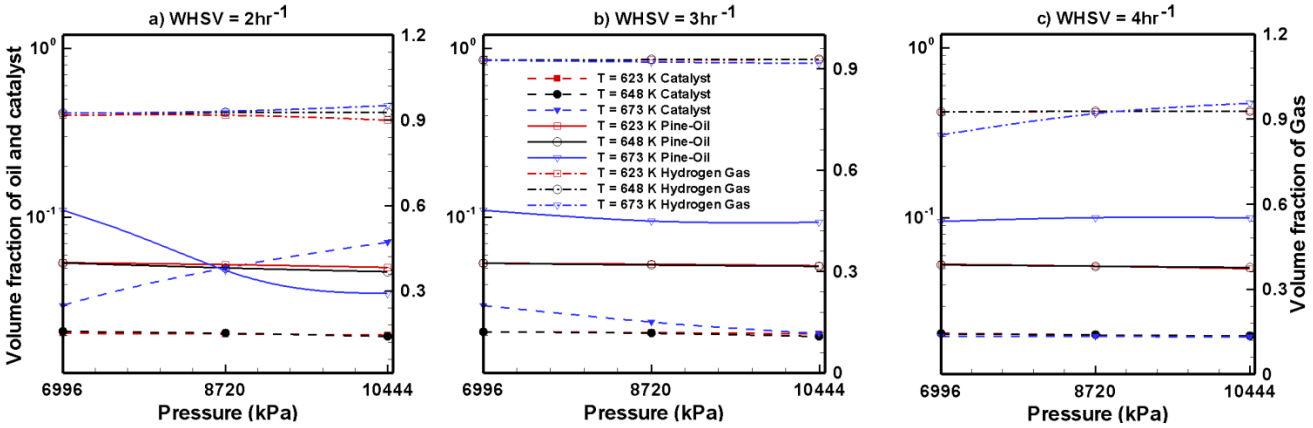

Fig. 7 Steady volume fractions of pine oil, H_2 gas and Pt/Al_2O_3 catalyst at different temperatures and pressures.

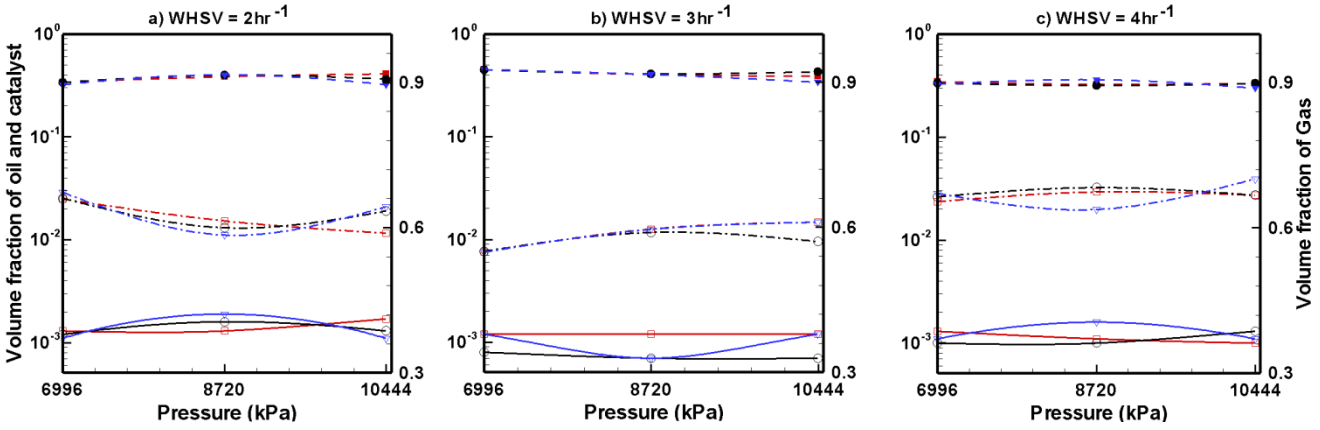

Fig. 8 Steady volume fractions of pine oil, H_2 gas and Ni-Mo/Al_2O_3 catalyst at different temperatures and pressures.

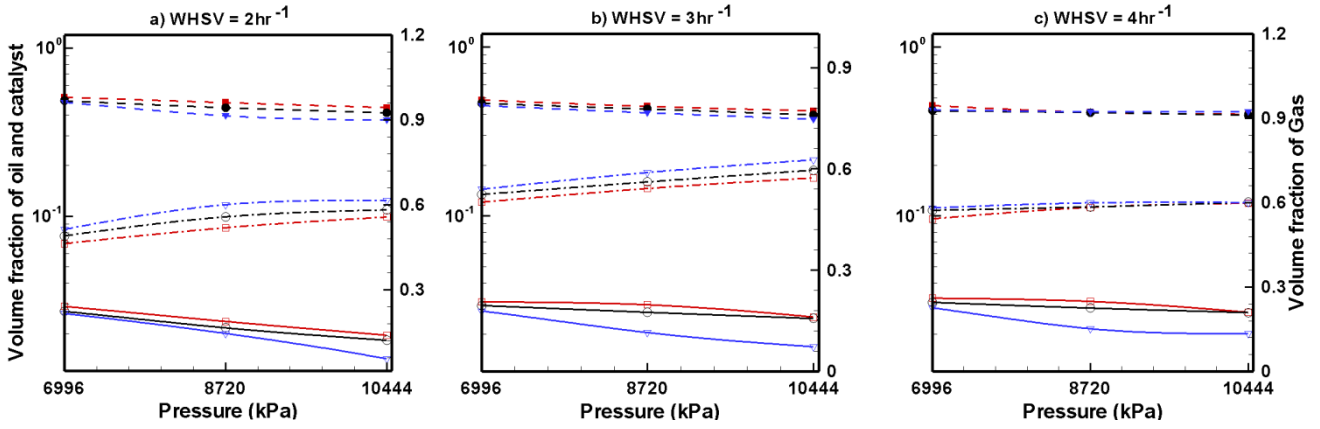

Fig. 9 Steady volume fractions of pine oil, H_2 gas and Co-Mo/Al_2O_3 catalyst at different temperatures and pressures.

In Figures 7-9, the left y-axis depicts the corresponding volume fraction values of pine oil and catalyst; and the right y-axis indicate the volume fraction values of the H_2 gas phase. It should be noted that the values of volume fraction of three phases presented in Figures 7-9 are steady state values, i.e., obtained after the bed has attained steady state by expanding up to the maximum attainable bed height. These volume fraction values also indicate that there is no further change in their values with the increasing time. Figure 7 shows the variations in the volume fraction of upgraded oil, H_2 gas and Pt/Al_2O_3 catalyst for different values of WHSV, temperature and pressure. The pine oil volume fraction shows mixed trend with respect to temperature and pressure at WHSV=2 hr^{-1} (Figure 7a); however at WHSV=3 hr^{-1} (Figure 7b) and WHSV=4 hr^{-1} (Figure 7c), it increases by increasing the temperature to T=673 K. But at fixed temperature, the volume fraction of pine oil is almost unaffected by the WHSV and pressure.

In the case of Ni-Mo/Al_2O_3 catalyst the variation in catalyst expansion behaviour is almost negligible with the change in WHSV, temperature and pressure (Figure 8). For the WHSV value of 2 hr^{-1} (Figure 8a), the steady volume fraction of H_2 gas slightly decreases with pressure at T=623 K; whereas at other temperatures, the volume fraction of H_2 gas shows mixed trend with the increasing pressure. By increasing the WHSV value to 3 hr^{-1} (Figure 8b), the volume fraction of H_2 gas at P=6996 kPa is unaffected by the temperature; however, as the pressure increases to P=8720 kPa and 10444kPa; mixed variations in volume fraction of H_2 gas is seen with the increasing temperature. By further increasing the WHSV to 4 hr^{-1} (Figure 8c), the volume fraction of H_2 gas at a given temperature and pressure has increased in comparison to the case of WHSV=3 hr^{-1} (Figure 8b). However, the volume fraction of H_2 gas shows mixed variations with respect to temperature and pressure in the case of WHSV=4 hr^{-1}. In the case of pine oil, the variations in their volume fraction with respect to temperature, pressure and WHSV values are very small and mixed behaviour is observed against changes in the operating conditions.

Figure 9 shows the volume fraction of upgraded bio-oil, H_2 gas and Co-Mo/Al_2O_3 catalyst for different WHSV, temperature and pressure values. The expansion of catalyst bed is almost unaffected

by WHSV, temperature and pressure. The volume fraction of H_2 gas slightly increases with the increasing pressure and with increasing temperature; however mixed trends of H_2 gas seen with respect to the WHSV values. The volume fraction of pine oil decreases with the increasing pressure and with the increasing temperature; however it increases with the increasing WHSV values when Co-Mo/Al_2O_3 catalyst is used. Finally, by comparing the performance of all catalysts (Figure 7-9), it can be seen that Pt/Al_2O_3 produces larger fraction of upgraded pine oil whereas Ni-Mo/Al_2O_3 produced smaller volume fraction of upgraded bio-oil.

Mass Fraction of Lumped Species of Upgraded Bio oil

Figures 10-11 show the steady mass fraction values of lumped species of upgraded bio-oil by HDO process in the presence of Pt/Al_2O_3 catalyst for different combinations of WHSV, temperature and pressure. The mass fraction values reported here in these figures are obtained when the bed has reached pseudo steady state. Figure 10 shows the steady mass fractions of lumped HNV and LNV in the presence of Pt/Al_2O_3 catalyst. At WHSV=2 hr^{-1} the steady mass fraction of LNV decreases slightly with the increasing pressure and with the decreasing temperature. At WHSV=3 hr^{-1}, the variation in mass fraction of LNV is negligible with changes in temperature and pressure. At WHSV=4 hr^{-1}, mixed variations in the steady state mass fractions of LNV are observed with respect to the temperature and pressure. The mass fractions of HNV at WHSV=2 hr^{-1} (Figure 10a) and WHSV= 4 hr^{-1} (Figure 10c) show mixed trend with respect to temperature and pressure; however at WHSV=3 hr^{-1} (Figure 10b), at a given temperature the mass fraction of HNV slightly decreases with the increasing pressure. The variation in mass fraction of HNV at WHSV=3 hr^{-1} (Figure 10b) and fixed value of pressure, has shown mixed trend with the temperature. From Figure 11a, it can be seen that the mass fractions of phenols and alkanes and aromatics show mixed trend with respect to the WHSV, temperature and pressure.

Figure 12 shows the variations in mass fraction values of lumped HNV and LNV species in the upgraded bio-oil by the HDO process in the presence of Ni-Mo/Al_2O_3 catalyst; and mixed trends can be seen here too with respect to WHSV, temperature and pressure. However compared to the case of Pt/Al_2O_3 catalyst (Figure 10) the mass fractions of HNV and LNV obtained by use of Ni-Mo/Al_2O_3 has substantially decreased for fixed combinations of WHSV, temperature and pressure.

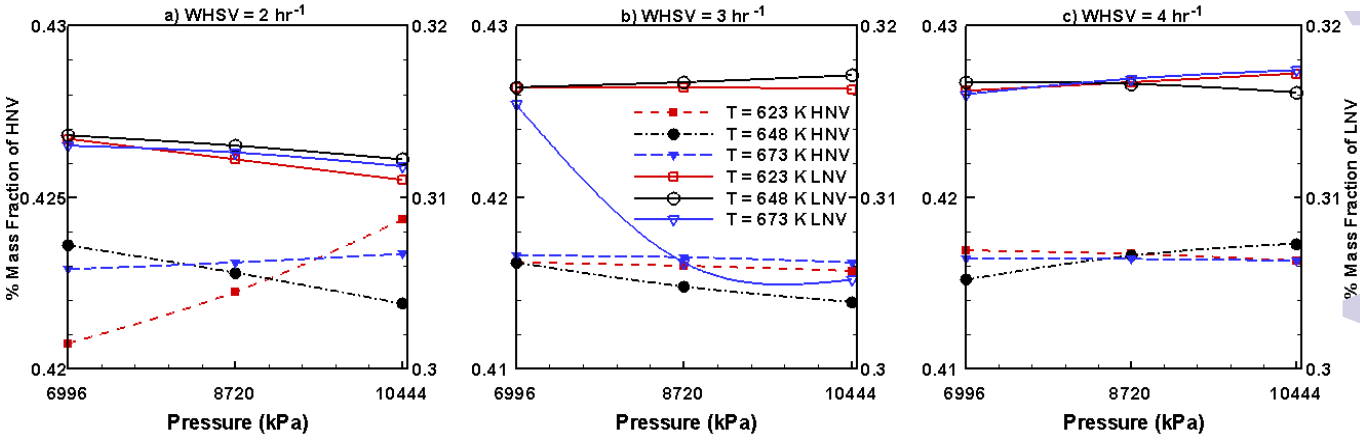

Fig. 10 Mass fractions of HNV and LNV obtained by upgrading the pine oil in the presence of Pt/Al_2O_3

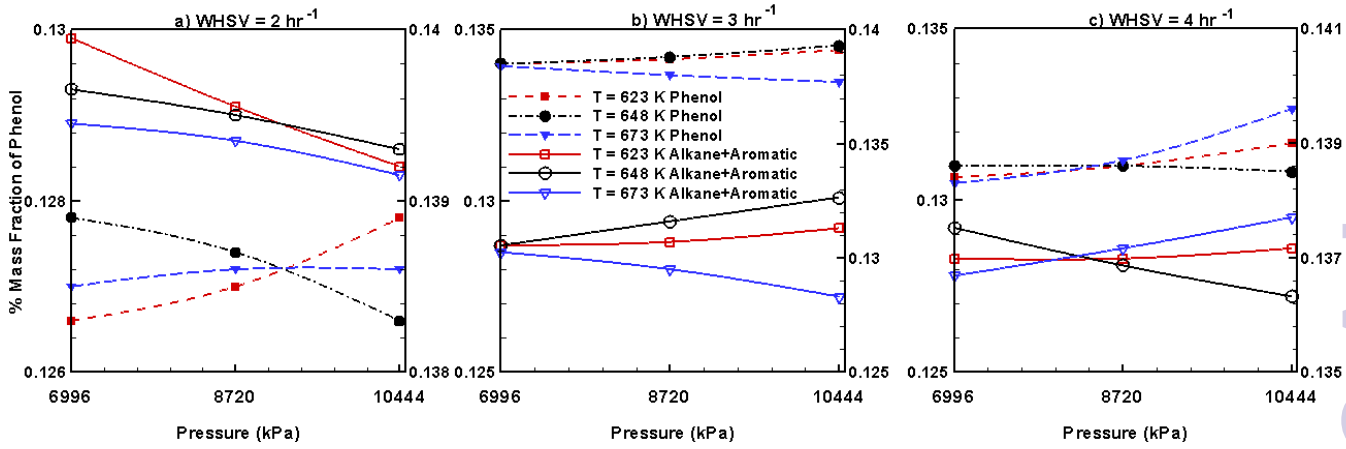

Fig. 11 Mass fractions of phenols and alkanes and aromatics obtained by upgrading the pine oil in the presence of Pt/Al_2O_3

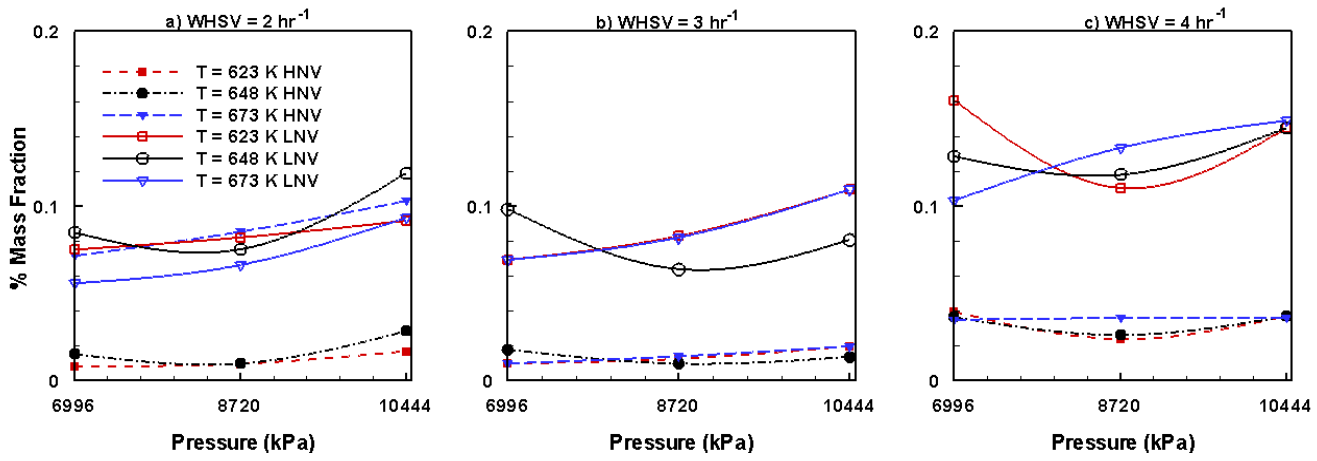

Fig. 12 Mass fractions of HNV and LNV obtained by upgrading the pine oil in the presence of Ni-Mo/Al_2O_3

Figure 13 shows the variations in the steady mass fractions of lumped phenols and alkanes and aromatics obtained by HDO of bio-oil in the presence of Ni-Mo/Al_2O_3; and mixed trends are seen with the changes in WHSV, temperature and pressure. However compared to the case of Pt/Al_2O_3 (Figure 11) the Ni-Mo/Al_2O_3 catalyst (Figure 13) produces larger mass fractions of phenols but smaller fractions of alkanes and aromatics.

Figure 14 shows the mass fractions of HNV and LNV obtained by the use of Co-Mo/Al_2O_3 catalyst. It can be seen from this figure that the mass fractions of both the HNV and LNV decrease with the increasing pressure, with the increasing temperature and with the increasing WHSV. In comparison to other catalyst, the Ni-Mo/Al_2O_3 produces small fractions of HNV and LNV followed by Pt/Al_2O_3 catalyst and Co-Mo/Al_2O_3 catalyst producing larger fractions of HNV and LNV. Figure 15 presents the mass fractions of phenols and alkanes and aromatics obtained by the use of Co-Mo/Al_2O_3 catalyst. It can be seen from Figure 15, that the formation of phenols by the use of Co-Mo/Al_2O_3 is almost unaffected by the temperature, pressure and WHSV values, however, the fractions of alkanes and aromatics increases with the increasing pressure, with the increasing temperature and with the increasing WHSV. By comparing with other two catalysts, the Co-Mo/Al_2O_3 catalyst produces larger fractions of alkanes and aromatics followed by Pt/Al_2O_3 and Ni-Mo/Al_2O_3 producing smaller fractions of alkanes and aromatics.

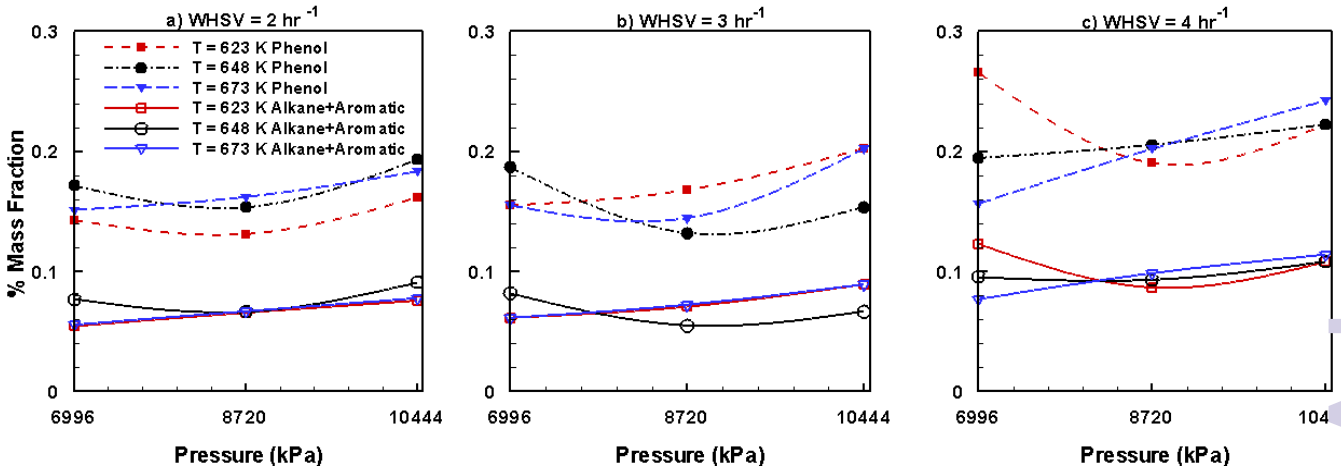

Fig. 13 Mass fractions of phenols and alkanes and aromatics obtained by upgrading the pine oil in the presence of Ni-Mo/Al_2O_3

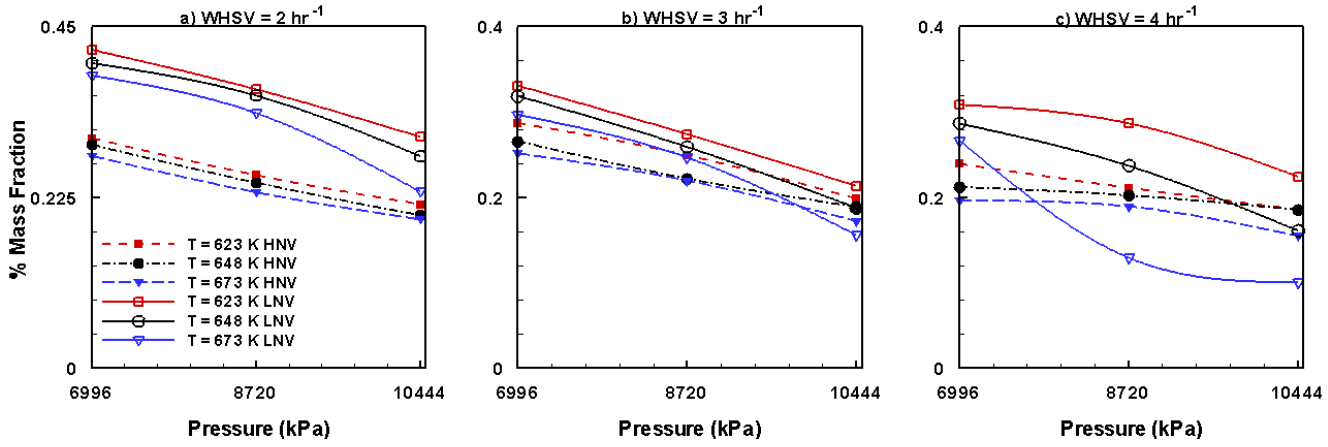

Fig. 14 Mass fractions of HNV and LNV obtained by upgrading the pine oil in the presence of Co-Mo/Al_2O_3

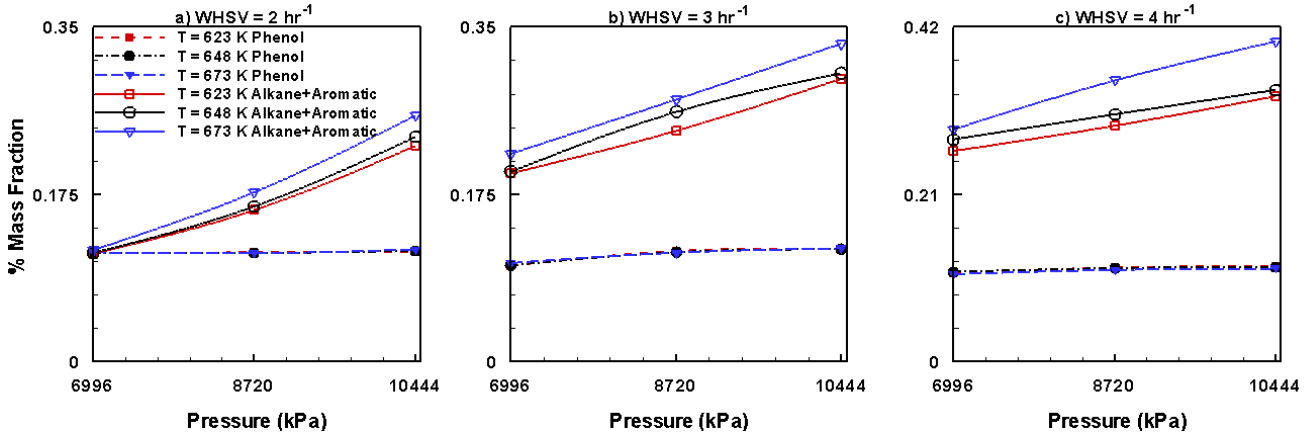

Fig. 15 Mass fractions of phenols and alkanes and aromatics obtained by upgrading the pine oil in the presence of Co-Mo/Al_2O_3

Conclusions

This numerical work presents the advancement of suitable catalyst for the upgradation of bio-oil through HDO process in an ebullated bed reactor at temperatures running between $623\ \mathrm{K} \leq \mathrm{T} \leq 673\ \mathrm{K}$, pressure ranges between $6996\ \mathrm{kPa} \leq \mathrm{P} \leq 10443\ \mathrm{kPa}$ and WHSV varying between $2 \leq \mathrm{WHSV}(\mathrm{hr}^{-1}) \leq 4$. The consequences of these studies demonstrate some important and significant behaviour of the three phases under the influence of three different catalyst namely alumina supported platinum, Co-Mo, and Ni-Mo catalysts. Some of the key findings of this study include the gas volume fraction is higher in the case of the Pt/Al_2O_3 catalyst. The amount of the phenol formation during the upgradation process is significant and effective in the case of the Ni-Mo/Al_2O_3 catalyst as compared to the other catalysts. The amount of the aromatics formation is larger by the use of the Co-Mo/Al_2O_3 catalyst in comparison with the other catalysts. The higher values of the volume and the mass fractions of upgraded lumped species are obtained at low WHSV values, and higher temperatures and pressures.

References

1. A. Oasmaa, D. Meier and A. Bridgwater, CPL Press: Newbury, UK, 2002.
2. E. Furimsky, Appl. Catal., A, 2000, **199**, 147.
3. J. D. Adjaye and N. N. Bakhshi, *Biomass Bioenergy,* 1995, **8**, 265-277.
4. K. L. Hew, A. M. Tamidi, S. Yusup, K. T. Lee and M. M. Ahmad, *Bioresour. Technol*., 2010, **101**, 8855-8858.
5. Z. Tang, L. Qiang, Z. Ying and G. Qingxiang, *Ind. Eng. Chem. Res*., 2009, **48**, 6923-6929.
6. Y. Zhang, W. Li, S. Zhang, Q. Xu and Y. Yan, *Chem. Eng. Technol*., 2012, **35**, 302-308.
7. A.V. Bridgwater, *Biomass Bioenergy*, 2012, 38, 68–94.
8. E. Furimsky, *Catal. Rev.: Sci. Eng*., 1983, **25**, 421.
9. S. T. Oyama, Blackie Academic and Professional: Glasgow Springer, 1996.
10. R. Maggi and B. Delmon, *Stud. Surf. Sci. Catal.,* 1997, **106**, 99.
11. O. Senol, Ph.D Thesis, Helsinki University of Technology, 2007.
12. F. H. Mahfud, Ph.D Thesis, University of Gronigen, 2007.

13. A. Gutierrez, M. E. Domine and Y. Solantausta, Co-processing of upgraded bio-liquids in standard refinery units-fundamentals, Berlin, 2007.
14. A. Gutierrez, R. K. Kaila, M. L. Honkela and R. Siloor, *Catal. Today*, 2009, 147, 239-246.
15. D. C. Elliott and T. R. Hart, *Energy Fuels*, 2009, **23**, 631-637.
16. US Pat., 4 795 851, 1989.
17. D. C. Elliott, *Energy Fuels*, 2007, **21**, 1792-1815.
18. D. C. Elliott, G. G. Neuenschwander and T.R. Hart, *ACS Sustainable Chem. Eng*., 2013, **1**, 389-392.
19. J. Wildschut, I. M. Cabrere and H. J. Heeres, Ind. Eng. *Chem. Res.,* 2009, **48**, 10324-10334.
20. J. Wildschut, M. Iqbal, F. H. Mahfud, I. Melian Cabrera, R. H. Venderborsch and H. J. Herres, *Energy Environ. Sci.,* 2010, **3**, 962-970.
21. N. Li and G. W. Huber, *J. Catal*., 2010, **270**, 48-59.
22. F. de Miguel Mercader, M. J. Groeneveld, S. R. A. Kersten, N. W.J. Way, C. J. Schaverien and J. A. Hogendoorn, *Appl. Catal., B,* 2010, **96**, 57-66.
23. E. Taarning, C. M. Osmundsen, X. Yang, B. Voss, S. I. Andersen and C. H. Chritensen, *Energy Environ. Sci.,* 2011, **4**, 793-804.
24. P. M. Mortensen, J. D. Grunwaldt, P. A. Jensen, K. G. Knudsen and A. D. Jensen, *Appl. Catal.,* A, 2011, **407**, 1-19.
25. Y. Wang, Y. Fang, T. He, H. Hu and J. Wu, *Catal. Commun.,* 2011, **12**, 1201-1225.
26. W. Baldauf, U. Balfanz and M. Rupp, *Biomass Bioenergy*, 1994, **7**, 237-244.
27. G. Fogassy, N. Thegarid, Y. Schuurman and C. Mirodatos, *Green Chemistry*, 2012, **14**, 1367-1371.
28. US Pat., 5 180 868, 1993.
29. T. Choudhary and C. Phillips, *Appl. Catal., A,* 2011, **397**, 1-12.
30. R.H. Venderbosch, A.R. Ardiyanti, J. Wildschut, A. Oasmaa, and H.J. Heeres, *J. Chem. Technol. Biotechnol*., 2010, **85**, 674–86.
31. E. Yaseen, C.A. Mullen, A.L.M.T. Pighinelli, and A. A. Boateng, *Fuel Process. Technol*., 2014, 123, 11–18.
32. J.P. Diebold, and J.W. Scahill, *Energy Prog.,1988,* **8**, 59-65.
33. E.M. Ryymin, M.L. Honkela, T.R. Viljava, and A.O.I. Krause, *Appl. Catal., A.,* 2010, **389**, 114–121.
34. C. Zhao, S. Kasakov, J. He, and J.A. Lercher, J. Catal., 2012, **296**, 12–23.
35. H.Y. Zhao, D. Li, P. Bui, and S.T. Oyama, *App Catal., A.*, 2011, **391**, 305–10.
36. Y. Zhao, L. Deng, B. Liao, Y. Fu, and Q. Xiang Guo, *Energy Fuels.* 2010, **24**, 5735–5740.
37. FLUENT Inc, *FLUENT User's Guide*, 2006.
38. J. Alder and T. E. Wainwright, *J. Chem. Phys*., 1960, **33**, 1439-1451.
39. D. Gidaspow, R. Bezburuah and J. Ding, *Proceedings of the seventh Engineering Foundation Conference on Fluidization,* Australia, 1992.
40. C. Y. Wen and Y. H. Yu, *Chem. Eng. Prog., Symp. Ser.,* 1966.
41. S. Ergun, *Chem. Eng. Prog.,* 1952, **48**, 89-94.
42. L. Schiller and Z. Naumann, *Z. Ver. Dtsch. Ing*., 1933, **77**, 318-320.
43. W. E. Ranz and W. R. Marshall, *Chem. Eng. Prog.,* 1952, **48**, 141-146.
44. D. J. Gunn, *Int. J. Heat Mass Transfer*, 1978, **21**, 467-478.
45. B. E. Launder and D. B. Spalding, Lectures in mathematical models of turbulence, Academic Press, London and New York, 1972.
46. J. Ding and D. Gidaspow, *AIChE J,* 1990, **36**, 523-528.
47. Y. H. E. Sheu, R. G. Anthony and E. J. Soltes, *Fuel Process. Technol*., 1988, **19**, 31-50.

Table of Contents

Effects of three catalysts on bio-oil upgradation using hydrodeoxygenation over a range of WHSV, temperature and pressure are numerically investigated using a CFD approach.